A spectro-astrometric study of southern pre-main sequence stars

Binaries, outflows, and disc structure down to AU scales

M. Takami[1], J. Bailey[2], and A. Chrysostomou[1]

[1] Department of Physical Sciences, University of Hertfordshire, Hatfield, Herts AL10 9AB, UK
[2] Anglo-Australian Observatory, PO Box 296, Epping, NSW 1710, Australia

Abstract. We present spectro-astrometric observations for 28 southern pre-main sequence (PMS) stars and investigate their circumstellar environment down to AU scales. The structures detected in the "position spectra" include: (1) almost all the known binary companions in our sample (Sz 68, Sz 41, HO Lup, VW Cha, S CrA, AS 205), (2) companion candidates which have not been detected by infrared speckle techniques (T CrA, MWC 300), (3) monopolar and bipolar jets (AS 353A, CS Cha), (4) a combination of jets and a bow shock (VV CrA), and (5) a combination of a jet and stellar companion (R CrA). Results in known binaries show that this technique is capable of detecting binaries with separations down to ~10 milliarcsec. Both components in each binary appear to have strikingly similar profiles in Hα emission, indicating a similarity of circumstellar activity (mass accretion and/or a wind), and supporting the scenario of core fragmentation for the mechanism of binary formation. The bipolar Hα jet in CS Cha has a spatial scale of ~1.5 AU, similar to that previously observed in RU Lup, and likely be heated by a mechanism other than shocks. From the spatial scale, velocity, and Hα luminosity, we estimate the mean hydrogen density in the AU-scale bipolar flows to be $\gtrsim 10^7$ cm^{-3}. The bipolar geometry in these jets can be explained by the presence of a disc gap/hole at AU scales, which could be induced by a gas-giant planet at the ice condensation radius.

Key words. accretion, accretion discs – line: formation – line: profiles – stars: activity – stars: evolution – stars: pre-main-sequence

1. Introduction

The circumstellar environment within 10 AU of young stars are of particular interest for star and planet formation. In this region, the star accretes the material from the circumstellar disc, and drives an energetic jet/wind (see, e.g., Najita et al. 2000; Shu et al. 2000; Königl & Pudritz 2000). In the circumstellar disc, planets would be growing up and tidally interact with the circumstellar environment (see e.g., Lubow & Artimowicz 2000). This region also includes a stellar companion in a significant number of objects, and the population, mass distribution, and orbital parameters of these companions could give useful constraints on the understanding of binary formation (see e.g., Mathieu et al. 2000). However, even the *Hubble Space Telescope* or adaptive optics on 10-m telescopes cannot resolve this region: a spatial scale of 10 AU corresponds to 0″.07 in the nearest star forming regions, which is comparable to the angular resolutions of these facilities. Observational studies in this region have thus been carried out by photometry and spectroscopy without any direct spatial information, and optical-to-radio interferometry in a limited number of objects.

To obtain spatial information well below these resolutions, we have begun "spectro-astrometric" observations of pre-main sequence (PMS) stars. Bailey (1998a) applied this technique for a PMS star, evolved star, and AGN, showing that the technique allows us to study the spatial structure of their emission/absorption features down to *milliarcsec* scales. Bailey (1998b) succeeded to detect almost all known PMS binaries in his sample, proving the potential of this technique to find new binaries with separations of well below 0.1 arcsec. Takami et al. (2001) then revealed the presence of bipolar structure at ~30 mas scale in the outflow of the T Tauri star RU Lup. This bipolar structure contrasts with the jet at larger scales, which exhibits only blueshifted components, suggestive of the presence of a disc gap at a few AU which allows the redshifted Hα outflow to be seen.

In this paper, we present results of spectro-astrometric observations for 28 southern PMS stars, and investigate their binarity, outflow activity, and disc structure down to AU scales. Section 2 summarizes the observations. Section 3 shows the detected structures due to stellar companions, jets, and bow shocks. Section 4 shows the Hα profiles for each component of known binaries, which probes the similarity or difference of circumstellar activities between binary components. Section 5 investigates the detectability of PMS binaries, the mechanism

of binary formation, physical conditions of the Hα outflows down to AU scales, and the possibility of planet formation in a few PMS stars. The conclusions of this paper is described in Sect. 6.

2. Observations

Observations were carried out at the 3.9-m Anglo-Australian Telescope using the RGO spectrograph. The configuration with a 1-arcsec slit width, a 1200 line mm^{-1} grating, and the 82-cm camera provided a spectral resolution ($\lambda/\Delta\lambda$) of 7000. The pixel scale of 0.15 arcsec with the MITLL CCD (2048 × 4096 deep depletion CCD from MIT Lincoln Labs) provides good sampling of the seeing profile, whose *FWHM* varies between 1 and 3 arcsec during the observations. The flat fields were made by combining many exposures with the spectrograph illuminated by a tungsten lamp. Wavelength calibration were made by observations of a CuAr lamp.

Table 1 shows the log of the observations. The targets were selected based on their brightness ($V \lesssim 14$), and most of them lie in the nearest low-mass star forming regions including Lupus (190 pc – Wichmann et al. 1998), Chamaeleon (170 pc – Bertout et al. 1999), Corona-Australis (130 pc – Marraco & Rydgren 1981), Ophiuchus (140 pc – de Geus & Burton 1991), and Upper Scorpius (150 pc – de Zeeuw et al. 1999). The spectra were obtained with a wavelength coverage of 6480–6780 Å (but 6140–6800 Å for VV CrA) to observe lines including Hα, [S II], He I 6678 Å, and obtained at four slit position angles (0°, 90°, 180°, and 270°) to determine the positional displacement in N–S and E–W directions. Although several targets were previously observed by Bailey (1998b), we observed them again to ensure all the data had uniform quality with which to carry out a statistical study.

The data were reduced using the FIGARO package provided by Starlink. After subtracting the bias level and flat-fielding, the position spectrum was determined by fitting the seeing profile at each wavelength with a Gaussian function. After the fitting, the position spectra with opposite position angles (0°–180°, or 90°–270°) were subtracted to remove instrumental effects (see Bailey 1998a,b; Takami et al. 2001 for detail). Each position spectrum has an arbitrary zero point, which we adjust to correspond to the continuum position. In addition to the position spectra, the intensity spectra were obtained by subtracting the bias, flat-fielding, subtracting the adjacent sky and extracting bright columns on the CCD. The systemic velocity of the targets was calibrated using photospheric absorption lines including Li I 6707.82 Å, N II 6613.62 Å, Ca I 6439.08 Å, Fe I 6475.63 Å, and Fe II 6456.38 Å.

The measured positional accuracy, σ, depends on the seeing size and the photon number at each wavelength. Each photon should be within a distance of the order of the seeing size from the actual position of the source, and this positional uncertainty is reduced by a factor of $N^{1/2}$ by observing N photons. Consequently, the detection limit is described as follows (Bailey 1998a):

$$\sigma(\text{milliarcsec}) = \text{const.} \cdot FWHM(\text{milliarcsec}) \cdot N^{-1/2}, \qquad (1)$$

where *FWHM* is the full width half maximum of the seeing. Table 1 provides the constant value of 0.5 ± 0.2, in agreement with that estimated using a Gaussian seeing profile (0.4). These results imply that the positional accuracies in our spectra are dominated by photon noise, other noise (e.g., readout noise) being negligible.

3. Positional displacement

Displacement in the position spectra of 12 objects were detected, including: (1) known binaries with separations of 0.1–1.5 arcsec (Sz 68, Sz 41, HO Lup, VW Cha, S CrA, and AS 205); (2) T CrA and MWC 300, whose displacement can be explained by a stellar companion; (3) CS Cha, AS 353A, and VV CrA, whose displacement can be attributed to outflowing gas; and (4) R CrA, whose displacement can be attributed to a combination of a stellar companion and outflowing gas. The following subsections describe the details for individual cases.

3.1. Known binaries (Figs. 1 and 2)

Among seven known binaries with separations of 0.1–1.5 arcsecs, displacement in Hα emission was detected in all of them but SR 20. Some of them also show displacement in other features including Fe II 6456 Å, Fe II 6516 Å, He I 6678 Å, and Li I 6708 Å.

The position angles and the angular scales of the displacement are summarized in Table 2. All the observed displacements lie at the binary position angle, and this tendency can be attributed to the two binary components having different spectra (Bailey 1998b). The exception is Hα emission in S CrA and AS 205, in which the direction of the displacement differs from the binary position angle beyond the 1-σ level. A likely explanation for S CrA is that the two binary components were not equally within the slit due to their wide binary separation. Indeed, infrared speckle observations give a binary separation of 1.4 arcsecs in this object, which is comparable to the seeing size for our observations (see Table 1). One might think that the observed difference of the position angle is due to orbital motion, although it is unlikely for the following reasons: (1) the binary position angle in S CrA increases with time (Bailey 1998b) while our results show a smaller position angle than previous measurements of the binary position angle by Ghez et al. (1997a), and (2) a central mass of 30–40 $M_\odot$ would be required to explain the difference between the two position angles, not plausible as a mass for a PMS star ($\lesssim 8$ $M_\odot$ – Stahler & Walter 1993). On the other hand, the different position angles in AS 205 can be explained by the orbital motion of the system. Indeed, the difference between the two position angles suggest a mass of the primary star of 2.4 $M_\odot$ assuming a circular orbit, consistent with that derived from the stellar luminosity and spectral type (1.5–2.5 $M_\odot$ – Liu et al. 1996).

The displacement of Hα emission/absorption in Sz 68, VW Cha, S CrA, and AS 205 show angular scales of 0.2–0.4 times as large as the binary separation, while it is much smaller in HO Lup and Sz 41 (0.01–0.02 as large as the binary separation). The latter results could be due to their large binary separations (~1.5 arcsec), in which the seeing of the brighter

Table 1. Log of the observations.

Object	HBC[a]	type[b]	V (mag)	Distance[c] (pc)	Date	seeing (″)	Photons[d] (×10⁴)	1-σ Detection Limit (mas)
SZ Cha	566	K0	12.0	170	1999.7.2	2.8	2	12.6
Th 12	605	M0	11.9	190	1999.7.2	2.1	6	2.9
MWC 300	–	B	10.5	1550	1999.7.2	<1.9[e]	4	3.6
T CrA[f]	290	F0	13.4	130	1999.7.2	<2.6[e]	4	4.6
S CrA	286	K6	11.1	130	1999.7.2	<2.9[e]	2	6.7
LkHα 332-20	244	K2	11.2	170	1999.7.3	1.2	9	1.3
CS Cha	569	K5	11.6	170	1999.7.3	1.2	8	1.6
Sz 77	603	M0	12.5	190	1999.7.3	0.9	8	1.5
SR 20	643	<K7	14.1	140	1999.7.3	1.4	2	3.9
LkHα 118	281	B5	11.1	–	1999.7.3	1.8	6	3.3
R CrA	288	A5	10.7	130	1999.7.3	4.5	2	15.3
LkHα 332-21	247	G8	11.0	170	1999.7.4	1.0	14	1.1
Sz 41	588	K0	11.6	170	1999.7.4	1.1	7	1.9
Sz 68	248	K2	10.3	190	1999.7.4	1.2	23	0.9
GQ Lup	250	K7	11.4	190	1999.7.4	1.3	7	2.1
VV Ser	282	B-A	11.9	440	1999.7.4	1.2	8	2.6
VV CrA	291	K7	13.0	130	1999.7.4	1.2	1	5.0
VW Cha	575	K2	12.5	170	2000.7.21	1.7	1	8.2
AS 205	254	K5	12.4	150	2000.7.21	2.0	2	5.6
TW Hya	568	K7	10.9	56	2000.7.21	1.3	4	2.2
AS 353A	292	–	12.5	300	2000.7.21	2.3	1	7.7
T CrA[f]	290	F0	13.4	130	2000.7.21	<2.6[e]	2	4.6
V4046 Sgr	–	–	10.5	–	2000.7.21	2.8	4	4.5
CU Cha	246	A0	8.5	170	2000.7.21	1.8	1–2	1.9
AS 209	270	K5	11.5	150	2000.7.21	2.6	3	4.6
HO Lup	612	M1	12.9	190	2000.7.23	1.1	0.5	6.7
CT Cha	570	K7	12.4	170	2000.7.23	1.3	2	2.5
BF Cha	–	–	–	170	2000.7.23	1.3	3	2.8
AS 206	259	K6-7	12.9	140	2000.7.23	1.4	1	5.8

[a] The number in the Herbig & Bell (1988) catalogue.

[b] References – Herbig & Bell (1988), Leinert et al. (1997).

[c] References – Bertout et al. (1999), de Geus & Burton (1991), de Zeeuw et al. (1999), Herbig & Jones (1983), Hillenbrand et al. (1992), Leinert et al. (1997), Marraco & Rydgren (1981), Whichmann et al. (1998).

[d] For each three pixels (corresponding to 0.4 Å) along the wavelength.

[e] These objects show asymmetric profiles, suggesting that a stellar companion contributes to the measured *FWHM*.

[f] This object was observe twice to investigate the time variation of the spatial structure reported by Bailey (1998a).

component does not include the flux from the fainter component. We thus conclude that angular scales for Hα emission in all the objects are consistent with those obtained in other pre-main sequence stars by Bailey (1998b): that is, 0.07–0.7. The displacement in most of the objects indicates the direction for one of the binary components, while that in the Hα profiles in S CrA and AS 205 lies in both directions: these profiles show central absorption and wing emission features, in which the position is displaced in the opposite directions.

The angular scales of the displacement in other emission/absorption lines are 0.02–0.05 per binary separation, much smaller than that in Hα emission. These small scales are attributed to smaller line-to-continuum ratios, which allow larger contribution of the continuum flux and reduce the positional displacement. In S CrA, the displacement indicates different directions between the lines: two Fe II lines lie in the direction of the primary, while He I and [S II] lines lie in the direction of the secondary.

Positional displacement of forbidden lines in PMS stars is often attributed to a jet/wind (e.g., Hirth et al. 1997; Takami et al. 2001, 2002), however, this explanation is not likely for the [S II] lines in S CrA. Indeed, optical polarization of T Tauri stars is very often perpendicular to jets within a few degrees (Ménard & Bastien 1992), although that in S CrA was measured to be 151–156 degree (Bastien 1985), nearly parallel to that of the positional displacement in the [S II] emission. We thus conclude that the displacement of the [S II] lines of S CrA is due to a binary companion.

3.2. T CrA (Fig. 3)

Infrared speckle observations by Ghez et al. (1997a) did not show the presence of a stellar companion, whereas the position spectra show displacement similar to that in known binaries, as first reported by Bailey (1998b). His and our results show angular scales for the displacement of 76 ± 5, 140 ± 9,
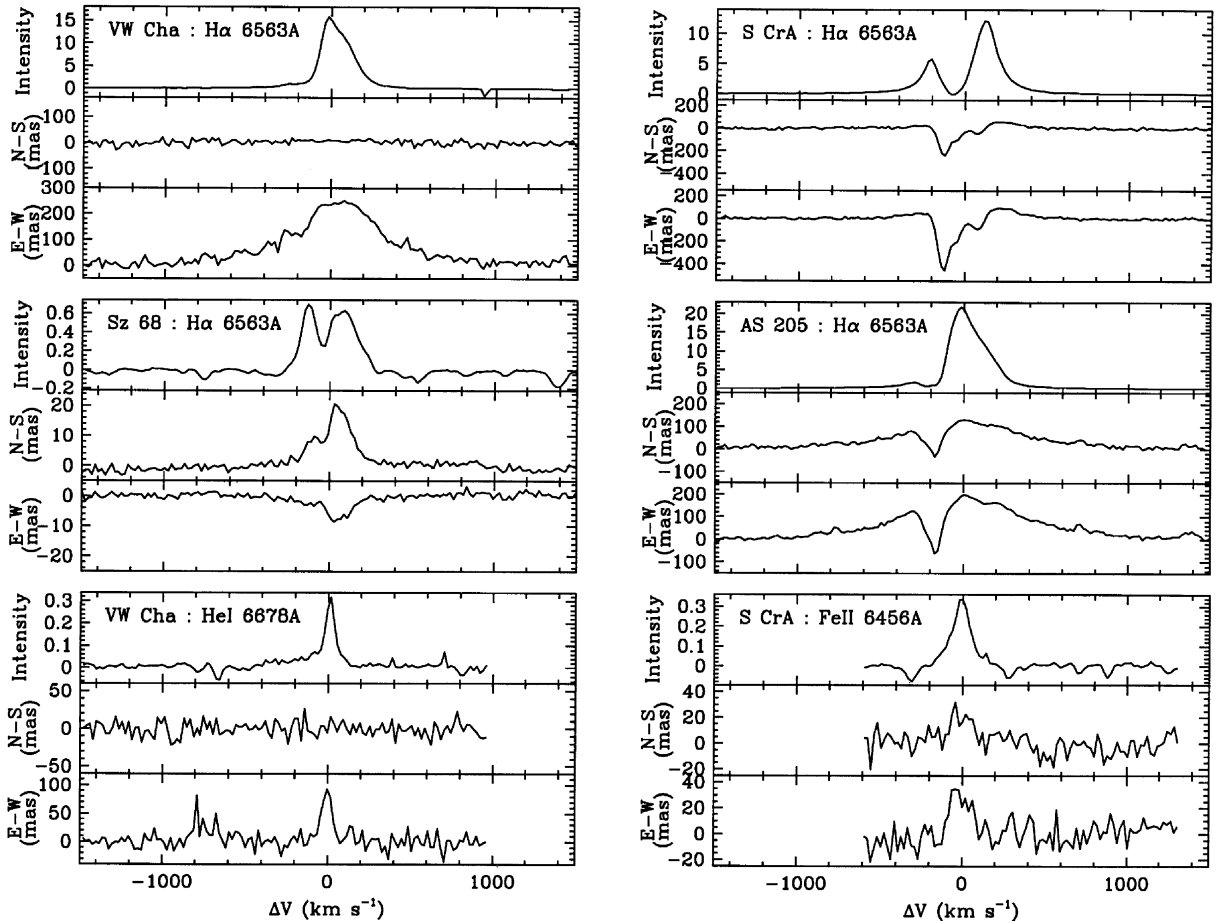
Fig. 1. Examples of intensity and position spectra for known binaries. Intensity spectra are normalized to the continuum.

122 ± 5, and 113 ± 3 milliarcsec in 1996, 1997, 1999, and 2000, respectively, indicating a lower limit for the binary separation of 140 milliarcsec. Such a separation is larger than the detection limit of infrared speckle, thus the non-detection of the companion by Ghez et al. (1997a) implies that the companion has a K-magnitude fainter than 10.5.

Figure 4 shows the position angles of the displacement measured in our four observing runs. The angle increases with time, corresponding to $\sim$2 degree/yr, consistent with the orbital motion of the stellar companion. From this result, we estimate a binary separation of $\sim$260 milliarcsec adopting a primary stellar mass of 0.8 $M_\odot$ (Hillenbrand et al. 1992) and assuming a circular orbit. In this case, the angular scales observed in the four runs would correspond to 0.29–0.54 per binary separation, consistent with those observed in known binaries (Sect. 3.1). On the other hand, time variation of the observed angular scale is not systematic as expected for binary motion, and such results could be attributed to variability of the emission feature between binary components (Bailey 1998b). Indeed, Hα emission observed by Bailey (1998b) and this work exhibit different shapes of profiles, supporting this explanation.

3.3. MWC 300 (Fig. 3)

Positional displacement was detected in the central absorption feature of the Hα emission, with an angular scale and a position angle of 17 ± 4 milliarcsec and $\sim$165°, respectively. Similar positional displacement was also observed in the known binary S CrA; thus, it is likely that the observed displacement in MWC 300 is due to a stellar companion. One might think that the observed displacement could be explained by a jet/wind, however, it is not likely since the displacement in this object is observed only at positive velocities, different from those expected in jets/winds (e.g., Takami et al. 2001, 2002), where the displacement is observed at negative or both velocities.

Previous infrared speckle observations failed to detect this companion (Leinert et al. 1997; Pirzkal et al. 1997). Corporon & Lagrange (1999) argue that MWC 300 is a spectroscopic binary, although our results cannot be explained as such: a combination of a lower limit for the binary separation provided by our results, the distance to the star (15.5 kpc – Leinert et al. 1997), and a typical mass of Herbig AeBe stars (5 $M_\odot$) suggests an orbital period of more than 2×10^3 yrs, much larger than the duration of the observations by Corporon & Lagrange (1999).

3.4. CS Cha (Figs. 3 and 5)

The displacement in Hα emission shows a bipolar structure: the blueshifted component extends towards the north-east while the redshifted component extends towards the south-west.
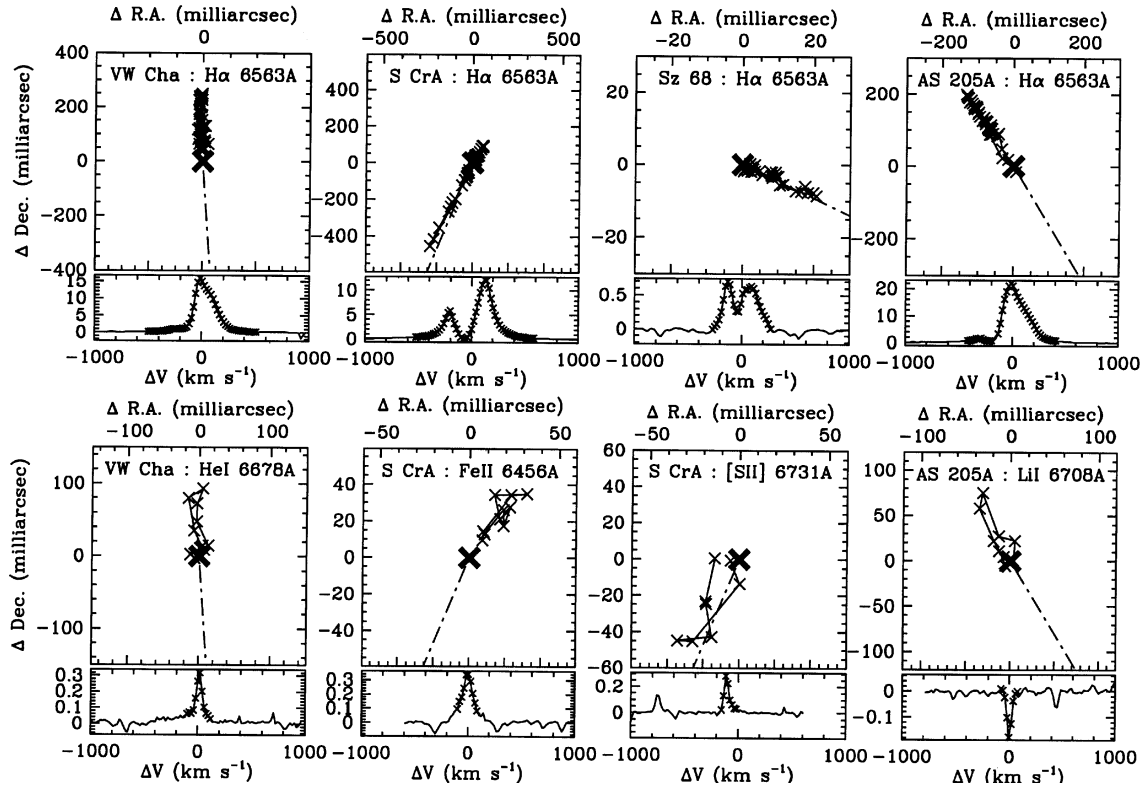
Fig. 2. Intensity profiles and positional displacement in emission/absorption features of known binaries VW Cha, S CrA, Sz 68, and AS 205. Small crosses in each map correspond to the velocity components shown in the intensity profile. A large cross in each figure indicates the centroidal position of the continuum source. A dot-dashed line indicates the direction of the fainter companion in the K-band continuum (Ghez et al. 1993, 1997a). The intensity profiles are normalized to the continuum.

The direction of the displacement is nearly perpendicular to that of the optical polarization (139° – Drissen et al. 1989), which is very often perpendicular to that of jets (Ménard & Bastien 1992, and references therein). Thus, it is likely that the bipolar structure in CS Cha is due to outflowing gas, as Takami et al. (2001) argue for RU Lup.

To determine the true spatial scale of the bipolar flow, we removed contamination by the continuum using the line-to-continuum ratio at each wavelength (see Takami et al. 2001 for detail), and plot the results in Fig. 5. The figure shows an angular scale of 8–10 milliarcsec, and asymmetric velocity field between the blueshifted and redshifted component: the displacement is observed at velocities of -100 to -20 km s^{-1} in the blueshifted component and $+100$ to $+250$ km s^{-1} in the redshifted component. The displacement along the outflow axis does not show clear positive correlation with the velocity as observed in RU Lup by Takami et al. (2001). Thus, the velocity field observed in this object cannot be simply attributed to the acceleration of the outflow, in which the displacement should increase with the velocity. Our result could be due to a contribution of magnetospheric mass accretion columns (see, e.g., Muzerolle et al. 1998, 2001) or an inner hot wind (Beristain et al. 2001; Alencar & Batalha 2002) to the observed Hα flux.

Forbidden lines in PMS stars often exhibit only blueshifted components due to obscuration of the counter flow by a circumstellar disc (Eislöffel et al. 2000, and references therein). On the other hand, Hα outflows in CS Cha have both blueshifted and redshifted components. This result can be explained if a gap or hole in the circumstellar disc allows the redshifted components to be seen (Takami et al. 2001). Indeed, the infrared spectral energy distribution (SED) in CS Cha shows no substantial excess emission less than 20 μm (Gauvin & Strom 1992), indicating a lack of dust with temperatures of more than 200 K. If we adopt a stellar luminosity of 2.7 $L_\odot$ (Gauvin & Strom 1992), this temperature corresponds to a disc radius of 6 AU, consistent with the spatial scale of the observed redshifted Hα outflow, i.e., $\sim$1.4 AU.

3.5. AS 353A (Fig. 3)

A positional displacement was observed within the blueshifted absorption of the Hα profile, at a velocity range between -200 and -300 km s^{-1}. This velocity coincides with that of the high-velocity component in the forbidden line profiles, peaking at -300 km s^{-1} (Hamann 1994) and considered to arise from a jet close to the star (Eislöffel et al. 2000 for review). In addition, the position angle of the displacement of $111 \pm 18°$ is coincident with that of a HH object associated with this star, HH 32C (103° – Solf et al. 1986). We thus conclude that a jet close to the star is responsible for the observed displacement. One might think that a binary companion could also explain the observed displacement, however, it is not likely since the emission component in the Hα profile does not show any displacement as observed in known binaries (see Sect. 3.1).
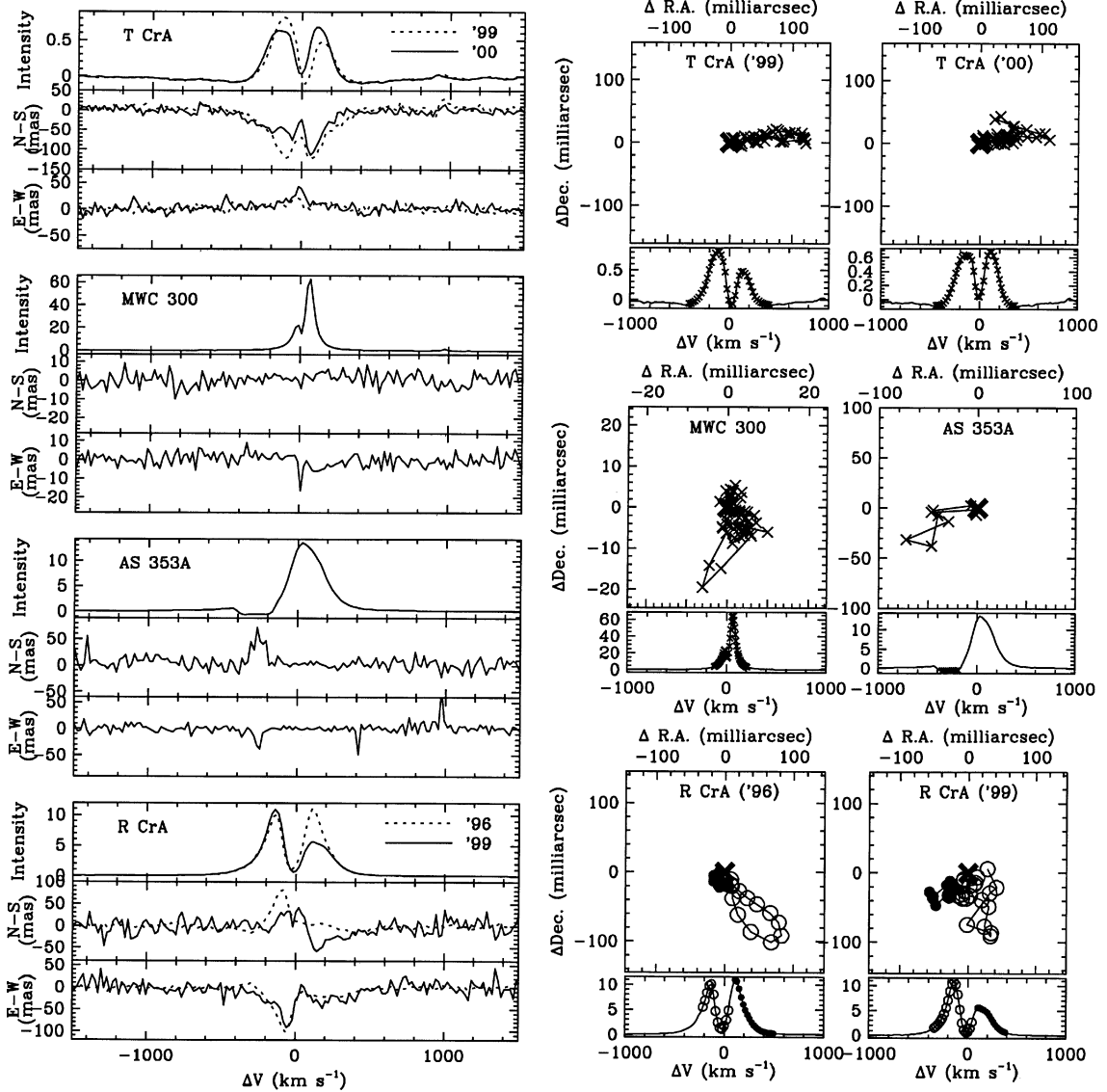
Fig. 3. Intensity profile and position displacement of the Hα emission in T CrA, MWC 300, CS Cha, AS 353A, and R CrA. The intensity profiles are normalized to the continuum. The results of R CrA in 1996 was obtained by Bailey (1998b).

Figure 3 shows that the displacement has an angular scale of 70 milliarcsec, corresponding to ~20 AU at the star. The inclination of the extended jet is measured to be 70° from the plane of the sky (Curiel et al. 1997); thus, the centroidal position of the emission line region is presumably located more than 60 AU apart from the star. Position spectra in this object do not show a displacement corresponding to the counterflow, as observed in RU Lup and CS Cha. Such results may be due to obscuration of the flow by a circumstellar disc, as observed in forbidden lines in many T Tauri stars.

3.6. R CrA (Fig. 3)

The positional displacement observed in Hα emission differs from any other objects described above. In 1996, the bluer component at −210 to 40 km s⁻¹ is displaced with an angular scale of 120 milliarcsec and at a position angle of ~220°, while the
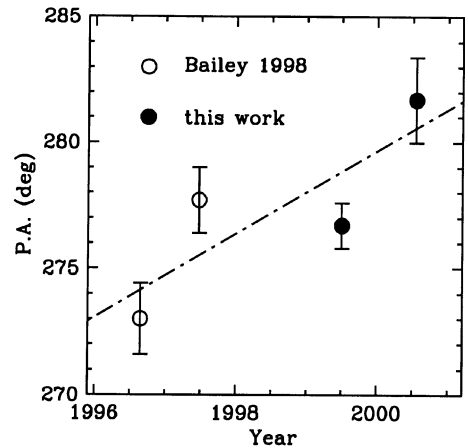

Fig. 4. Position angles of the displacement measured in T CrA. A dot-dashed line shows the regression line with an inclination of 1.65° yr⁻¹.

Table 2. Positional displacement in known binaries.

object	separation[a] (mas)	PA[a] (deg)	line		observed angular scale (milliarcsec)	(per binary separation)	observed PA (deg)
Sz 68	107 ± 7	245 ± 7	Hα	6563 Å	21 ± 1	0.20	248.2 ± 0.9
Sz 41	1500 ± 800	150 ± 20	Hα	6563 Å	22 ± 3	0.01	186 ± 3
HO Lup	1490 ± 70	35 ± 2	Hα	6563 Å	24 ± 9	0.02	213 ± 1
VW Cha	660 ± 30	184 ± 2	Hα	6563 Å	250 ± 12	0.38	2.5 ± 0.5
			He I	6678 Å	93 ± 12	0.14	4 ± 3
S CrA	1410 ± 60	157 ± 2	Hα	6563 Å	513 ± 9	0.36	153.1 ± 0.3
					111 ± 9	0.08	331.1 ± 0.5
			Fe II	6456 Å	47 ± 9	0.03	323 ± 3
			Fe II	6516 Å	49 ± 9	0.03	338 ± 4
			He I	6678 Å	57 ± 9	0.04	150 ± 5
			[S II]	6716 Å	31 ± 9	0.02	146 ± 2
			[S II]	6731 Å	57 ± 9	0.04	148 ± 3
AS 205	1317 ± 2	211.87 ± 0.08	Hα	6563 Å	239 ± 8	0.18	33.5 ± 0.4
					67 ± 8	0.05	202 ± 4
			Fe II	6456 Å	61 ± 8	0.05	36 ± 3
			Fe II	6516 Å	60 ± 8	0.05	37 ± 2
			He I	6678 Å	34 ± 8	0.03	34 ± 4
			Li I	6708 Å	81 ± 8	0.06	28 ± 3

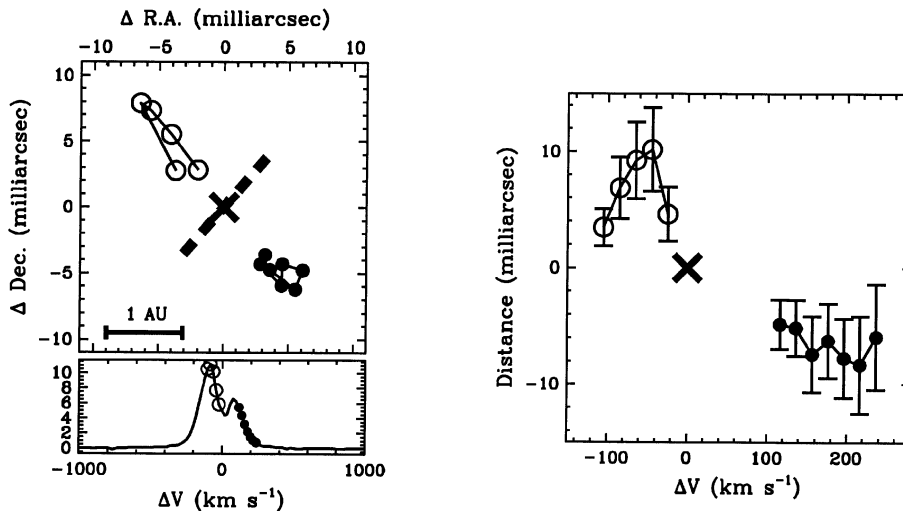[a] Observed by Ghez et al. (1995, 1997a).

Fig. 5. (Left) Spatial distribution of positional displacement in Hα emission of CS Cha. Contamination by the continuum was removed using the line-to-continuum ratio at each wavelength: thus, the plot shows the true angular scale of the Hα emission. Open and filled circles show blue- and redshifted components, respectively, and each circle in the map corresponds to that in the intensity profile shown below. A large cross and a dashed bar at the centre show the centroidal position of the continuum and the direction of optical polarization, respectively. The scale of the profile is normalized to the continuum flux. (Right) Correlation between velocity and radial distance of the displacement. A large cross shows the centroidal position of the continuum.

redder component at 110 to 600 km s^{-1} does not show clear displacement. In 1999, the position of these components are displaced at position angles of ~200° and ~130° with angular scales of 100 and 70 milliarcsecs, respectively. Neither a stellar companion or a monopolar/bipolar outflow can explain these results.

Such results could be explained by a combination of two companions, or that of a stellar companion and an outflow. However, the former explanation is not likely for the following reason. Recent surveys show that young multiple systems are invariably hierarchical: i.e., with different orbital scales by a factor of at least 3 and typically more than 10 (e.g., Simon et al. 1995; Ghez et al. 1997a; Köhler et al. 2000). This implies that two stellar companions cannot simply explain our results in R CrA, in which displacement in two directions show similar angular scales. A combination of a stellar companion and an outflow is thus more likely to explain the observed displacement. Emission lines from outflows often exhibit only blueshifted components (e.g., Hirth et al. 1997): thus, a likely explanation is that the displacement in the bluer emission is

due to an outflow, while that in the redder emission is due to a stellar companion.

Hillenbrand et al. (1992) estimate a primary stellar mass of 0.8 $M_{\odot}$ in this object, and our results provide a lower limit for the binary separation of 8 AU. These parameters provide the timescale of the orbital motion of more than 24 yr, much larger than the duration of our observations. This fact suggests that the observed time variation in the redshifted emission is due to the variation of the spectra in two binary components, as observed in T CrA (Sect. 3.2), rather than binary motion.

3.7. VV CrA (Fig. 6)

Positional displacement was observed in Hα and several forbidden lines, and these are attributed to the following three flows: (1) flow A, which appears in the [S II] and [O I] emission at velocities of −100 to 20 km s^{-1}; and (2) flow B, which appears in the [N II] and [S II] emission at velocities of −270 to −100 km s^{-1}; (3) flow C, which appears in the [O I] and Hα emission at velocities of −350 to −200 km s^{-1}. The position in the flow monotonically changes with velocity in the [S II] emission of flow A and B, and that in the [O I] line in flow C.

The displacement in the lowest velocities of flow A is associated with the primary star shown in Fig. 6, indicating that the flow is driven by the star at the centroidal continuum position. The [S II] profiles exhibit distinct components at high and low velocities, as observed in many other stars, and the latter component is located within 0.2 arcsec of the star, corresponding to a spatial scale of <25 AU. This spatial scale is similar to those observed in other T Tauri stars (e.g., Hirth et al. 1997; Takami et al. 2001, 2002), supporting the idea that the flow is driven by this PMS star. On the other hand, in flow B, the displacement at the lowest velocities lies in the north-east, in the direction of a companion with a separation of 2 arcsec (Graham 1992; Reipurth & Zinnecker 1993; Ghez et al. 1997a). Thus, it is likely that flow B is driven by this companion, known as an "infrared companion" (Koresko et al. 1997). The [NII] emission in this flow is located further from this star than the [SII] lines, as observed in small-scale jets in many other T Tauri stars (Hirth et al. 1997), and such results support this conclusion.

Previous infrared observations by Graham (1992) and Ghez et al. (1997a) do not show the presence of a young star associated with flow C. In this flow, the [O I] line has a width of a few hundred km s^{-1}, suggesting the coexistence of shocks with different velocities. In addition, the line with a higher excitation energy, Hα, arises from the highest velocities. These results can be attributed to a bow shock in which the Hα and [O I] emission arise from its apex and wakes, respectively. The extension of the [O I] emission suggest that the driving source lies in the west, in which a few IRAS sources were identified by Wilking et al. (1992), although it is located far (>2 arcmin) from VV CrA. Thus, the driving source of flow C is not clear.

4. Hα profiles in binary components

We can derive the intensity spectrum for each component of known binaries from the intensity and position spectra, the

binary separation measured by infrared speckle techniques, and an assumed continuum flux ratio (see Bailey 1998a; Garcia et al. 1999). The centroidal position of the seeing in a PMS binary is described as follows:

$$\mathbf{x}_\lambda = \frac{I_{\lambda(\mathrm{prim})}}{I_\lambda}\boldsymbol{x}_{(\mathrm{prim})} + \frac{I_{\lambda(\mathrm{sec})}}{I_\lambda}\boldsymbol{x}_{(\mathrm{sec})},$$

or

$$\Delta d_\lambda = \frac{I_{\lambda(\mathrm{sec})}}{I_\lambda}d, \tag{2}$$

where $\boldsymbol{x}_\lambda$ is the centroidal position of the seeing, and $\boldsymbol{x}_{(\mathrm{prim})}$ and $\boldsymbol{x}_{(\mathrm{sec})}$ are positions of the primary and the secondary stars, respectively; I_λ, $I_{\lambda(\mathrm{prim})}$, $I_{\lambda(\mathrm{sec})}$ are intensities of the whole system, the primary star, and the secondary star, respectively; Δd_λ is the separation between the primary star and the centroidal position of the seeing; d is the binary separation projected on the sky. Positional displacement in an emission/absorption feature is measured relative to the centroidal position of the continuum emission, thus its spatial scale is described as follows based on Eq. (2):

$$\Delta d'_\lambda = \Delta d_\lambda - \Delta d_{\mathrm{cont}} = \left(\frac{I_{\lambda(\mathrm{sec})}}{I_\lambda} - \frac{I_{\mathrm{cont(sec)}}}{I_{\mathrm{cont}}}\right)d, \tag{3}$$

where $\Delta d'_\lambda$ is the observed displacement in a position spectrum; Δd_{cont}, I_{cont} and $I_{\mathrm{cont(sec)}}$ are the distance to the centroidal continuum position from the primary star, the total luminosity of the continuum, and that of the secondary star, respectively. From this equation, the flux from each star is obtained as follows:

$$\begin{aligned} I_{\lambda(\mathrm{sec})} &= \left(\frac{I_{\mathrm{cont(sec)}}}{I_{\mathrm{cont}}} + \frac{\Delta d'_\lambda}{d}\right)I_\lambda = \left(\frac{f}{1+f} + \frac{\Delta d'_\lambda}{d}\right)I_\lambda, \\ I_{\lambda(\mathrm{prim})} &= I_\lambda - I_{\lambda(\mathrm{sec})}, \end{aligned} \tag{4}$$

where f is the continuum luminosity of the secondary star relative to the primary.

Figure 7 shows the profiles of the Hα emission obtained from Eq. (4) for six of our objects with known separation. Despite the uncertainty of the continuum flux ratio, the figure shows that the two binary components have strikingly similar profiles to each other – similar linewidths and the absorption feature at similar velocities. The figure also shows that the line-to-continuum ratio is higher at the secondary than the primary in all the objects. Although the profiles in HO Lup do not clearly show this tendency, the observed positional displacement lies in the direction of the fainter component (Reipurth & Zinnecker 1993), agreeing with this conclusion. These results also imply that the position of the Hα feature in all the objects is primarily displaced in the direction of the component fainter at optical wavelengths.

5. Discussion

5.1. Detectability of close (<0.1 arcsec) binaries using spectro-astrometry

Recent high-resolution techniques, such as infrared speckle observations and the *Hubble Space Telescope*, have revealed
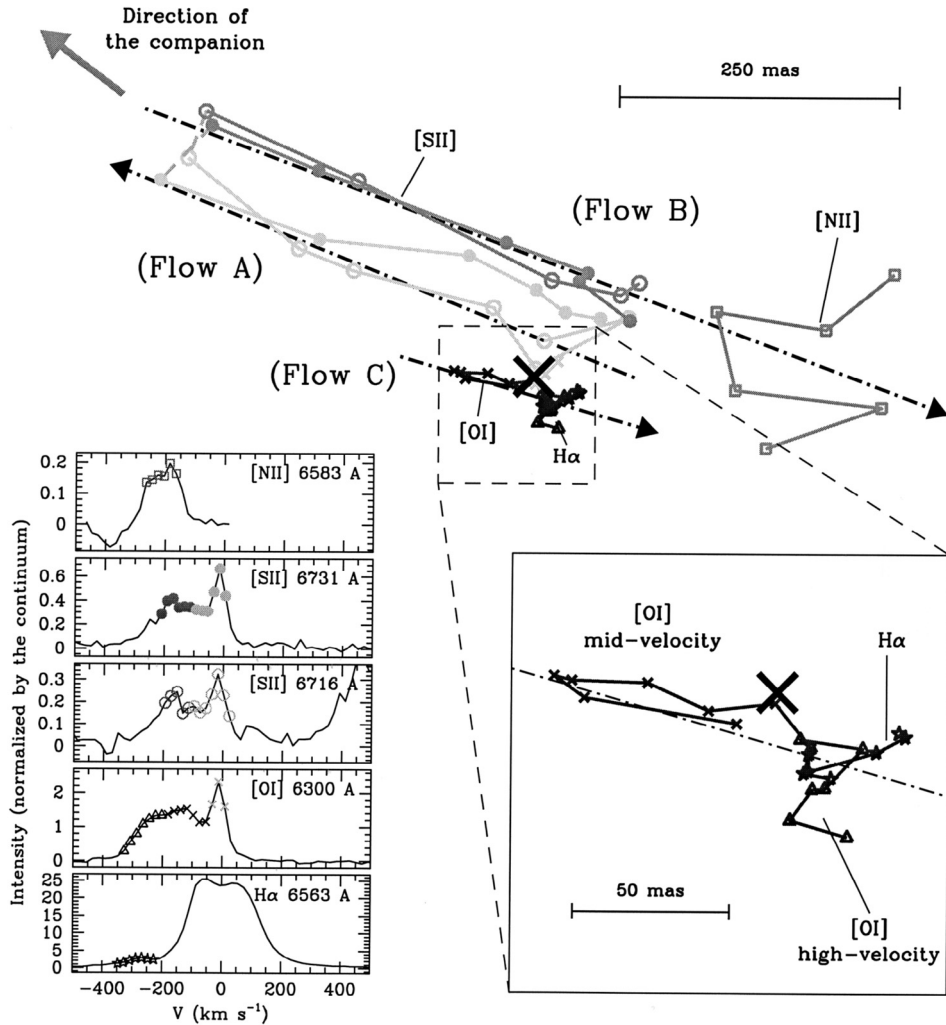
Fig. 6. Positional displacement in VV CrA. Contamination by the continuum is removed as carried out for Fig. 5. Small open squares, filled and open circles, and stars correspond to velocity components in the profiles of [N II] 6583 Å, [S II] 6731 and 6716 Å, and Hα, respectively, at the bottom-left of the figure. Small open triangles and crosses are those for [O I] 6300 Å but different velocities – −330 to −200 km s^{-1} and −180 to 10 km s^{-1}, respectively. Different grey tones indicate the displacement in flow A–C, respectively (see the text for detail). A large cross shows the centroidal position of the continuum. The dot-dashed arrows show the variation of the velocities in the flows from low to high values. The displacement in [O I] 6363 Å is not plotted, since it is consistent with that in [O I] 6300 Å, which has the same upper transition level. The intensity profiles in the bottom-left of the figure are normalized to the continuum.

a difference in binary populations between star-forming regions. These observations show that the binary frequencies in low-mass star-forming regions are higher than that of solar-type field stars with the same range of binary separation (e.g., Ghez et al. 1993; Leinert et al. 1993; Ghez et al. 1997a). Alternatively, the frequency appears to be similar to that of the field stars in a massive star-forming region, the Orion Trapezium cluster (Prosser et al. 1994; Padgett et al. 1997; Petr et al. 1998). Such a different binary population between regions could be caused by initial conditions, such as stellar density or cloud temperature (see Mathieu et al. 2000 for review).

However, the traditional observing techniques have not been able to cover the complete range of binary separations in various star-forming regions. Direct imaging and infrared speckle have allowed detection of PMS binaries down to separations of ~100 milliarcsec, corresponding to ~15 AU with periods of 50 years or more in the nearest star-forming

regions. On the other hand, spectroscopic measurement has been capable of detecting binaries with periods of a few days and separations of well under an AU. These techniques cannot cover the intermediate separations (0.1–10 AU), leading to significant incompleteness. Lunar occultations have explored this gap in some cases, however, this technique can measure the separation only in one-dimension in the sky, and applies for a limited number of star-forming regions as well as relying on chance occultations.

Spectro-astrometric observations by Bailey (1998b) and this work suggest that this technique is capable of discovering PMS binaries with these intermediate separations. These observations detect 10 out of 12 known binaries with separations of 0.07–1.5 arcsec, and a few new binary candidates which have not been detected using other techniques. The observed angular scales in known binaries (0.07–0.7 times as large as the binary separation – Sect. 4) and positional accuracy achieved
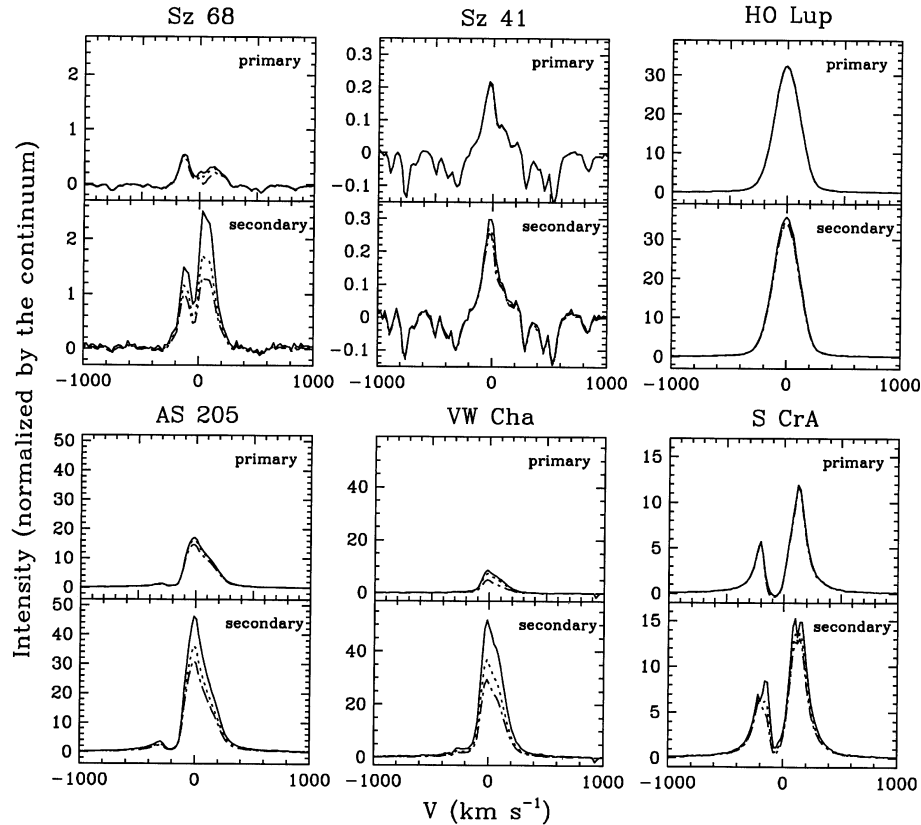
Fig. 7. Profiles of the Hα emission for each binary component of known binaries Sz 68, Sz 41, HO Lup, AS 205, VW Cha, and S CrA. Solid, dot, and dot-dashed profiles were obtained by assuming the flux ratios of $f = 0.2$, 0.4, and 0.8, respectively, at the continuum level. In this figure, the "primary" and "secondary" components are defined based on the continuum flux at 6500–6800 Å, different from Fig. 2 and Table 2. The intensity scale is normalized to the continuum for each binary component.

(down to 1 milliarcsec) suggest that the technique should be able to detect binaries with separations down to ∼10 milliarcsec at the 3-σ level. This detection limit is comparable to that of lunar occultations (see Richichi et al. 1994; Simon et al. 1995), although spectro-astrometry can easily achieve better limits by detecting a larger number of photons (see Eq. (1)), and applies for objects with any coordinate and binary position angles.

Equation (3) shows that the detectability of binaries using this technique depends on the line and continuum flux ratios between binary components. In addition, the position spectra in Hα emission show different shapes from the intensity profiles (see Fig. 1), indicating that the detectability also depends on a slight difference in the line profiles for the primary and secondary stars. These facts may be susceptible to more complicated selection effects than those of direct imaging, infrared speckle, and lunar occultations. To investigate this effect, we plot the relation between the angular scale of the displacement, Hα equivalent width of the whole system, and relative K magnitude between binary components in Fig. 8. The figure shows that the displacement has no correlation with the Hα equivalent width, while there is a clear correlation with the relative K magnitude. These results suggest that our technique has a selection effect similar to those of infrared speckle (Ghez et al. 1993) and lunar occultations (Simon et al. 1995); i.e., dependent on the relative K magnitude and independent of the line flux. The latter correlation between the displacement and

relative K magnitude can be explained as follows: if the secondary star has a bright stellar/disc luminosity, it is likely to have bright Hα emission (see Cabrit et al. 1990) and bright K band emission, thereby providing a small difference in the K magnitude from that of the primary and a large displacement in Hα emission towards the secondary.

From the regression line in Fig. 8, we estimate the detection limit of binary separation using our technique as a function of the relative K magnitude (Fig. 9). The same figure also shows binary parameters discovered by lunar occultations with separations of less than 0''.1 (Richichi et al. 1994, 1996, 1997; Simon et al. 1995). The figure indicates that we could detect 90% of binaries discovered by lunar occultations, and our detection limit appears to be slightly better than that of the lunar occultation method for both binary separation and relative K magnitude. Such a high sensitivity for relative K magnitude is also followed by a discovery of a companion candidate in T CrA, which Ghez et al. (1997a) failed to detect despite a sufficient separation (>0.14 arcsec – see Sect. 3.2).

In two separated studies, we failed to detect the companions in T Tau (Bailey 1998b) and SR 20 (this work), which were detected by Ghez et al. (1993) using infrared speckle. The non-detection for the former object could be due to the fact that the secondary star is an "infrared companion" and faint at optical wavelengths (Koresko et al. 1997). Such companions form only ∼10% (White & Ghez 2001) or less (Ghez et al. 1997a;
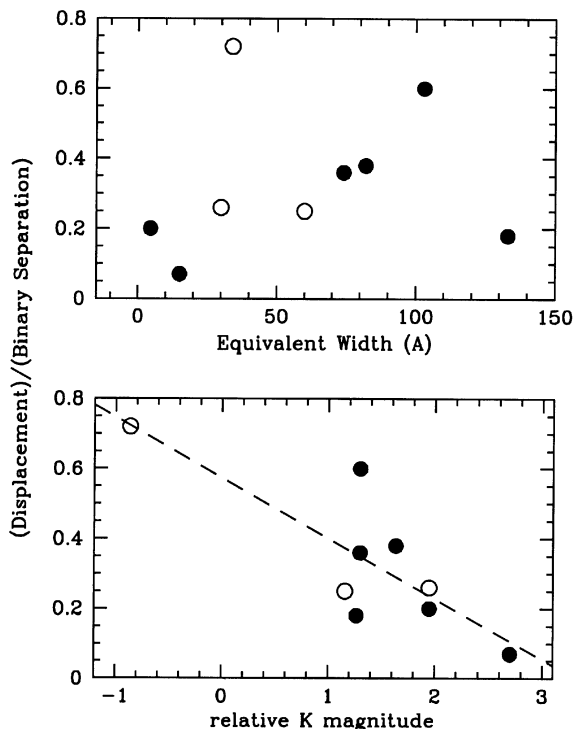
Fig. 9. The detection limit of PMS binaries using spectro-astrometry. The hatched area shows the parameter space in which we can *not* detect binaries exceeding the 3-σ level. This limit is estimated assuming a positional uncertainty of 1 mas in the position spectra. The filled and open circles, and crosses show the binaries discovered by lunar occultations by Simon et al. (1995), Richichi et al. (1994), and Richichi et al. (1996, 1997), respectively.

Fig. 8. Relation between the angular scale of the displacement and Hα equivalent width of the whole system (upper), and relative K magnitude between binary components (lower). The open and filled circles show the results for Herbig Ae/Be stars and classical T Tauri stars, respectively. The regression line (dashed) is shown in the lower figure. Data for the displacement and Hα equivalent widths are obtained from Bailey (1998b) and this work, while the relative K magnitudes are obtained from previous infrared speckle observations by Ghez et al. (1993), Ghez et al. (1997a), and Leinert et al. (1997).

5.2. Binary frequency in our sample of the nearest southern star-forming regions

The observed targets shown in Table 1 include 22 PMS stars in nearby (130–200 pc) star-forming regions: including 7 known binaries with separations of 0.07–1.5 arcsec (Sect. 3.1), and two "spectro-astrometric" binaries in T CrA (Sect. 3.2) and R CrA (Sect. 3.6). Among these binaries, R CrA may have a separation of less than 0.1 arcsec, corresponding to ≲15 AU. In contrast, lunar occultations surveys by Simon et al. (1995) detected 8 binaries out of 47 PMS stars in Taurus and 5 out of 35 PMS stars in Ophiuchus at these short (≲15 AU) separations. Is the binary frequency at these separations smaller in our sample than the Taurus and Ophiuchus star-forming regions?

To investigate this, we determine the binary frequency of our sample. We exclude SZ Cha from this statistical study due to a remarkably low detection limit (13 mas). The objects in which a companion has not been detected have a typical uncertainty in their measured displacement of 3 milliarcsec. Given that the typical observed angular scale per binary separation is 0.3 for Hα emission (see Sect. 3.1 and Table 1), this implies that a companion has not been detected down to 30 milliarcsec (3σ), equivalent with ∼5 AU in the observed star-forming regions. Table 3 shows binary populations in our sample with two different separation ranges (15–300 AU and 5–15 AU), together with those in various star-forming regions and field stars. An accurate binary separation is not known for R CrA, and this fact is included in the uncertainty of the tabulated values. The table shows that our sample has a larger binary frequency for separations of 15–300 AU than that in field stars. Such a result is consistent with those derived in other low-mass star-forming regions. On the other hand, all the frequencies tabulated for the shorter separations have large statistical uncertainties, implying that the provided separation range is insufficient to investigate the difference of binary frequencies between star-forming regions. Observations of 60 stars with an uncertainty of 1 mas in

Köhler et al. 2000) of the entire PMS population. Another possible explanation for non-detection is that Hα emission is faint or absent at the companion of T Tau and SR 20, thereby not allowing the positional displacement towards the secondary. Again, such binary systems may not significantly affect the entire population for PMS binaries: recent observations have shown that companions of classical T Tauri stars (CTTSs) are usually CTTSs, and a combination of a CTTS and a weak-line T Tauri star (WTTS) is rare (≲20% – Prato & Simon 1997; Duchêne et al. 1999).

All the results described above suggest that we can improve the previous statistics of PMS binary populations using spectro-astrometry. Note that most of the known binaries in our sample have bright Hα emission ($EW_{H\alpha} > 10$ Å), implying that the detection of PMS binaries using our technique could be efficient only for such objects as CTTSs. Indeed, Eq. (3) suggests that the displacement could be shorter for binaries with small line-to-continuum ratios. Although Fig. 8 does not show such a tendency, it could appear if we included the objects with fainter Hα emission. This fact implies the detectability of binaries using our technique could be worse for objects such as WTTSs.
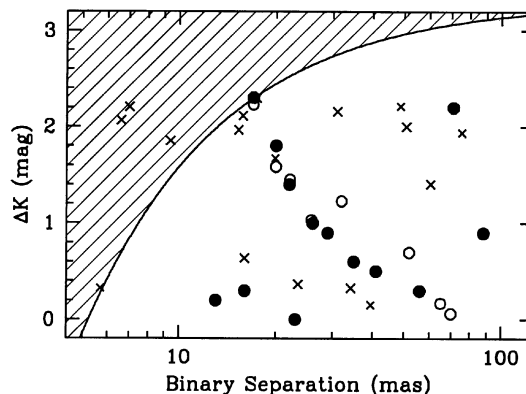
Table 3. Binary population in star-forming regions.

separation = 15–300 AU[a]		
region	binary fraction	reference
Taurus	0.37 ± 0.09	Ghez et al. (1993)
	0.32 ± 0.08	Simon et al. (1995)
Ophiuchus	0.14 ± 0.06	Simon et al. (1995)
Oph-Sco	0.29 ± 0.12	Ghez et al. (1993)
Sco-Cen	0.26 ± 0.05	Köhler et al. (2000)
Cha/Lup/CrA	0.31 ± 0.08	Ghez et al. (1997a)
field stars	0.16 ± 0.04[b]	DM91[c]
our sample in southern SFRs	0.41 ± 0.16	this work

separation = 5–15 AU[a]		
region	binary fraction	reference
Taurus	0.06 ± 0.04	Simon et al. (1995)
Ophiuchus	0.06 ± 0.04	Simon et al. (1995)
field stars	0.06 ± 0.02[b]	DM91[c]
our sample in southern SFRs	0.05 ± 0.05	this work

[a] Assuming the distance of all the star-forming regions of 150 pc for simplicity.
[b] Adopting the factor by Leinert et al. (1993) to convert the orbital period to the separation.
[c] Duquennoy & Mayor (1991).

their position spectra could allow us to investigate it in detail: we could detect 8 ± 3 companions with these separation ranges if the binaries in the observed regions had the same number distribution of separations as that in solar-type main-sequence stars observed by Duquennoy & Mayor (1991).

5.3. Implications for the binary formation mechanism

Approximately two-thirds of all solar-type main-sequence stars are members of multiple systems (Duquennoy & Mayor 1991), and it may be even higher in low-mass star-forming regions (see Mathieu et al. 2000). Despite the apparent ubiquity of binaries, astronomers have not yet identified the primary mechanism by which they form. Possible formation mechanisms include (see Hartigan et al. 1994a; Ghez et al. 1997b): (1) fragmentation of a collapsing molecular core, (2) gravitational instability in an equilibrium disc, and (3) dynamical capture. The secondary mass distribution in field stars is remarkably similar to the mass function of primary stars with low-to-high masses (Fischer & Marcy 1992; Duquennoy & Mayor 1991; Abt et al. 1990), supporting protostellar "capture" as the mechanism by which binaries form. On the other hand, stellar ages, infrared excess, and emission line features in PMS binaries indicate that these are at the same evolutionary stage, supporting the scenario of core fragmentation (e.g., Hartigan et al. 1994; Ghez et al. 1997b; Prato & Simon 1997; Duchêne et al. 1999; White & Ghez 2001).

Our results in Sect. 4 show that the two binary components have strikingly similar Hα profiles to each other. Such results contrast to a rich variety of profiles among PMS stars

(see Reipurth et al. 1996). The variety of these profiles is due to interplay between the accretion flow and a wind closest to the source: thus, our results suggest that the two binary components tend to have similar flow geometry and velocity for mass accretion/ejection. Such results could exclude the scenario of dynamical capture and disc instability for binary formation, since (1) capture would provide a rich variety of profiles even between binary components, and (2) disc instability could provide different evolutionary stages between binary components, thereby providing different inflowing/outflowing activities. Our results thus support the scenario of core fragmentation for binary formation, as well as other studies for PMS binaries

Accretion flows and/or winds in YSOs are likely to have non-spherical geometry (Shu et al. 2000; Königl et al. 2000; Najita et al. 2000): thus, the similarity of the Hα profiles observed in binary components would also require the condition that the axes of the inflows/outflows are aligned with each other. Such a condition is consistent with a previous polarimetric study by Monin et al. (1998), who show that the position angles of polarization are preferentially parallel in PMS binaries. On the other hand, Hale (1994) shows that the orbital and equatorial planes appear to be randomly distributed in main-sequence binaries with separations more than 30–40 AU. Such a difference between PMS and main-sequence binaries could result from different formation mechanisms, or different initial conditions of the protostellar core. In the latter case, the results in PMS binaries could come from the pre-collapse material all rotating around a single axis, while those in main-sequence binaries could originate from an the initial cloud core in which the angular momentum distribution has strong spatial variations (see the discussion of Bate et al. 2000).

5.4. Physical conditions of jets down to AU scales

The results for the Hα outflows obtained by Bailey (1998b), Takami et al. (2001) and this work are summarized in Table 4. Among these objects, three of them are known as active PMS stars: Z CMa and AS 353A are associated with extended jets (e.g., Poetzel et al. 1989; Solf et al. 1986) and RU Lup shows an extremely high accretion luminosity (3–6 $L_\odot$ – Lamzin et al. 1996). Such high activities have not been explicitly reported for CS Cha, although the object shows high variability in Hα emission: measured equivalent widths range from 13 Å (Herbig & Bell 1988) to 54 Å (Reipurth et al. 1996) and 60 Å (this work), and the observed line profile in Fig. 5 show a different shape from that observed by Reipurth et al. (1996).

The velocities of blueshifted Hα outflows in RU Lup, Z CMa, AS 353A coincide with those of the high-velocity components in forbidden lines: −100 to −250 km s^{-1} in RU Lup (Takami et al. 2001); −600 to −800 km s^{-1} in Z CMa (Corcoran & Ray 1997); −200 to −350 km s^{-1} in AS 353A (Hamann 1994). This forbidden line emission is considered to arise from jets close to the star (see Eislöffel et al. 2000, and references therein): thus, this coincidence of velocities suggests that the Hα emission in these objects also arises from jets close to the source. Although the Hα emission in PMS stars are often

Table 4. Summary of Hα outflows.

object	projected scale (AU)	velocity[a] (km s^{-1})	$EW^a_{H\alpha}$ (Å)
RU Lup	~5[b]	$-200 \leq v \leq -50$ $200 \leq v \leq 300$	29.7
CS Cha	~1.5	$-100 \leq v \leq -20$ $100 \leq v \leq 250$	28.3
Z CMa	>70[c]	$-700 \leq v \leq -50$	_[d]
AS 353A	>20	$-300 \leq v \leq -200$	_[d]

[a] Sum for the blueshifted and redshifted emission in which positional displacement is observed.
[b] Larger than that in Takami et al. (2001) due to the updated distance (Wichmann et al. 1998).
[c] Adopting the distance of 1150 pc provided by Clariá (1974).
[d] Equivalent widths cannot be derived since the displacement is overlapped with the absorption feature.

considered to arise from the magnetospheric accretion columns, these results are not surprising for the following reasons. First, the idealized magnetospheric accretion models by Muzerolle et al. (1998, 2001) failed to reproduce permitted line profiles in active PMS stars, suggesting that the presence of another contributor to the emission. In addition, dozens of YSOs exhibit thermal radio emission, which is likely due to the ionized gas in jets close to the source (see Anglada 1996). From the Hα luminosities in RU Lup and CS Cha, we can derive upper limits of the thermal radio luminosities of 0.1–0.4 mJy kpc^2 at 3.6 cm (see Appendix A), consistent with those observed in other Class II objects (see Beltrán et al. 2001)[1].

Hα emission-line regions in Z CMa and AS 353A show spatial scales more than 50 AU (see Table 4 and Sect. 3.5), and there is growing evidence that the jets at these scales are heated by shocks in the internal working surfaces. Recent high-resolution imaging of PMS stars exhibit knotty, bubbly, and bow-shape structures in jets at these scales (e.g., Kepner et al. 1993; Bacciotti et al. 2000; Dougados et al. 2000). Lavalley-Forquet et al. (2000) carried out a detailed analysis of line ratios in DG Tau, and reach the conclusion that the jet is heated by shock, and not ambipolar diffusion nor turbulent viscosity in the mixing layer. Their conclusion is supported by Takami et al. (2002), who discover He I 1.083 μm emission in the same jet: only shocks could explain the presence of such a high-excitation (~20 eV) line.

On the other hand, the same heating mechanism cannot simply explain the following results in RU Lup and CS Cha. Hα emission in these objects show spatial scales of 1–5 AU, much smaller than the distance between internal working surfaces observed in PMS jets (≳100 AU – see, e.g., Ray et al. 1996; Dougados et al. 2000). In addition, their line profiles do not exhibit a peak at the velocity of the jets, and indicate that Hα emission in these jets is continuously distributed

[1] We assume that the magnetospheric accretion columns do not significantly contribute to the radio flux due to its large optical thickness and small size, or obscuration by an optically thick jet/wind. The latter explanation is often used for the fact that WTTSs often show nonthermal radio emission from the magnetosphere, while it is usually absent in CTTSs and Class I YSOs (see, e.g., André et al. 1992; Martin 1996).
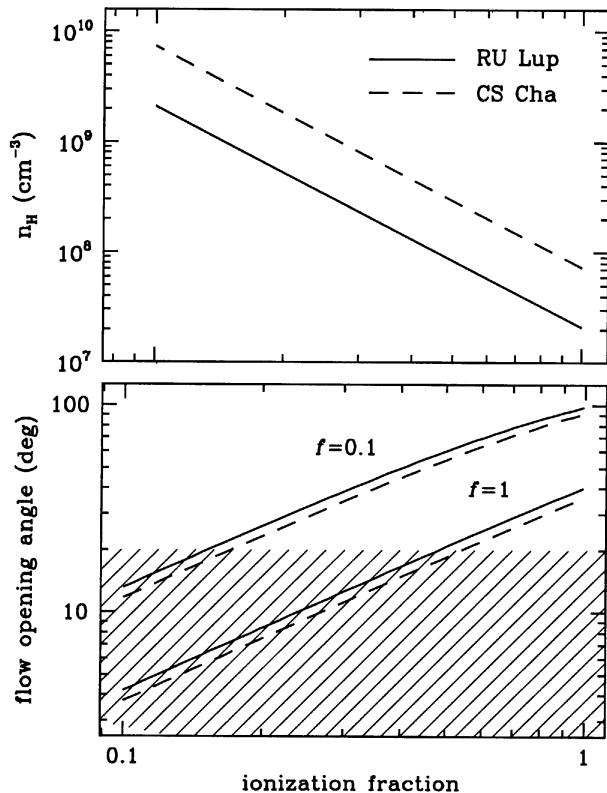
from the accelerating region. These results suggest the presence of another heating mechanism in the inner (<10 AU) region, which could be (1) X-ray heating (Shang et al. 2002); (2) MHD-wave (e.g., Hartmann et al. 1982); (3) ambipolar diffusion (Safier 1993; Garcia et al. 2001); (4) turbulent dissipation in a viscous mixing layer (Binette et al. 1999); or (5) UV photoionization. Among these mechanisms, ambipolar diffusion and viscous mixing layer models provide a lower ionization fraction than shocks, as indicated by the predicted [NII]/[OI] line ratios (see Lavalley-Fouquet et al. 2000). Such a prediction is inconsistent with the spatial distributions of Hα and [OI] emission in RU Lup, which indicates a higher ionization fraction in the inner region than for the outer region heated by shocks. PMS stars often exhibit UV continuum excess as a result of mass accretion (see e.g., Calvet et al. 2000), although this could also be rejected for the following reason. The hot continuum emission of RU Lup at >1200 Å is approximately fitted by a blackbody with a temperature of 6.8–7.8×10^3 K and a luminosity of 2.7–6 $L_\odot$ (Lamzin et al. 1996), and a flux of ionizing photons of 10^{37}–10^{38} s^{-1} from this region could sustain only 10^{-4}–10^{-3}% of the recombination rate corresponding to the observed Hα luminosity. Thus, one of the remaining two mechanisms, X-ray or MHD-wave heating, would be more likely for the heating mechanism in this region. The same mechanisms are also proposed for magnetospheric accretion columns, which are responsible for Balmer and other permitted lines in many PMS stars (Lamzin et al. 1996; Calvet & Gullbring 1998).

From the spatial scales, flow velocities, and Hα luminosities, we can estimate the typical hydrogen number densities and opening angles in these AU-scale outflows. The details of the calculation is described in Appendix B. Throughout we assume the following: (1) an electron temperature of 10^4 K, (2) viewing angle of 45°, (3) $\dot{M}_{\rm out} = 0.1 \times \dot{M}_{\rm acc}$, where $\dot{M}_{\rm out}$ and $\dot{M}_{\rm acc}$ are the mass loss rate and mass accretion rate, respectively, and (4) the flow has axisymmetric geometry and zero width at its origin. The first assumption is based on models which include X-ray heating (Shang et al. 2002) or the temperature of magnetospheric accretion columns (e.g., Muzerolle et al. 2001), in which the presence of MHD-wave heating is suggested by Calvet & Gullbring (1998). The second assumption is likely to be a good approximation for order-estimates, since viewing angles close to pole-on and edge-on would not provide the observed displacements and velocities, respectively. The third assumption is based on Calvet (1997), who revised the estimate from forbidden line and accretion luminosities by Hartigan et al. (1995). For mass accretion rates in RU Lup and CS Cha, we adopt 7.7×10^7 and 1.6×10^7 $M_\odot$ yr^{-1}, respectively, obtained by John-Krull et al. (2000).

Figure 10 shows the derived hydrogen number densities and opening angles in RU Lup and CS Cha, as a function of the assumed ionization fraction. The upper figure shows that the hydrogen number density is ≳10^7 cm^{-3} for any case, and larger for lower ionization fractions. Previous imaging observations have shown that opening angles of jets are likely to be ≳20° within ~100 AU of the stars (see Eislöffel et al. 2000, and references therein; see also Bacciotti et al. 2000), and the lower figure shows that this fact gives lower limits to the

Fig. 10. Mean hydrogen density and flow opening angle as a function of the ionization fraction. The estimated opening angle depends on the volume filling factor in the flow, which are assumed to be 0.1 and 1. The hached area indicates unlikely opening angles (see the text).

ionization fraction of 0.2–0.5 for the assumed volume filling factors of 0.1–1, providing the upper limits of $n_H \sim 10^9$ cm^{-3}.

5.5. Disc gap/hole in CS Cha and RU Lup – Implications for planet formation

Recent radial velocity surveys have revealed a number of extrasolar giant planets (see, e.g., Marcy et al. 2000). These observations show a population minimum between stellar-substellar companions and extrasolar giant planets ("the brown dwarf desert" – Marcy et al. 2000; see also Halbwachs et al. 2000), suggesting the presence of another formation mechanism for the planetary-mass objects. The proposed mechanisms include: (1) core accretion via accumulation of dust grains, which is generally accepted and requires 10^6–10^7 yrs for planet formation (e.g., Pollack et al. 1996), and (2) disc instability, which could form a gas giant planet only in a few hundred years (Boss 2000).

Model calculations have shown that a young planet could tidally interact with a circumstellar disc, opening up a gap or hole at its orbital scale (see Lubow & Artymowicz 2000; Takeuchi et al. 1996). Even the most recent high-resolution techniques cannot resolve such AU-scale structures in the nearest star-forming regions, while infrared spectral energy distributions (SEDs) in several young stars exhibit dips at the mid-infrared, suggesting the presence of such gaps/holes (e.g., Strom et al. 1989; Marsh & Mahoney 1992, 1993). However,

recent studies by Boss & Yorke (1993, 1996) show that the SEDs cannot provide convincing proof for the presence of a disc gap or hole as these dips could also be caused by a combination of vertical temperature structure and changes in dust opacity.

On the other hand, our results for RU Lup (Takami et al. 2001) and CS Cha (this work) are providing evidence for the presence of disc gaps/holes at AU scales. These objects exhibit the presence of Hα bipolar jets at AU scales, and the detection of the redshifted flows is explained by a disc gap/hole allowing this flow to be seen (Takami et al. 2001; Sect. 3.4). Our position spectra would also be capable of discovering a stellar companion. No evidence for companion is seen, suggesting that the gap and hole in these objects could be induced by unseen companions.

The SEDs suggest that the outer radii of the gap and hole correspond to a temperature of ~200 K, coincident with the ice condensation temperature (160–200 K – see Marsh & Mahoney 1992; Boss 1995). Marsh & Mahoney (1992, 1993) also obtained similar temperatures from mid-infrared dips in GK Tau and HK Tau SEDs for which stellar companions have not been detected. In contrast, the gaps/holes induced by a stellar companion show a wide range of temperatures: Guilloteau et al. (1999) provide an inner temperature of the GG Tau ring of ~30 K, while results by Jensen & Mathieu (1997) suggest temperatures up to ~600 K in the gaps/holes towards spectroscopic binaries. Marsh & Mahoney (1992, 1993) suggest that such results could be explained if a gas-giant planet formed at the ice condensation radius and clearing up the innerside of the circumstellar disc by tidal interaction. Indeed, theoretical work shows that the formation time scales of the gas-giant planets are likely to be shorter at the ice condensation radius or outer region than the inner region: the presence of water ice could enhance the surface density of the solid material by a factor of 3–4 (e.g., Hayashi 1981), providing a shorter timescale for the planetesimal accretion (Lissauer 1987). Furthermore, water vapor produced in the inner region could condensate at the ice condensation radius, enhancing the surface density of ice by a factor of ~70 (Stevenson & Lunine 1988), thereby allowing the ice condensation radius to be a preferential location for formation of giant planets.

RU Lup, CS Cha, GK Tau, and HK Tau have stellar ages of 1–3×10^6 yr (see Palla & Stahler 1999 for the evolutionary tracks, and Lamzin et al. 1996; Gauvin & Strom 1992; and Marsh & Mahoney 1993 for their effective temperatures and luminosities), implying that the young planets could be formed within this timescale. This result contrasts with the detailed simulations by Pollack et al. (1996), who suggest that ~5 × 10^6 yr is required for the formation of a Jupiter in the solar nebula. This age problem could be overcome if the initial surface density is higher than their standard model (10 g cm^{-2} for solid material at the scale of the Jovian orbit). These authors show that the timescale for the formation of giant planets appears to be extremely sensitive to the initial surface density of the protoplanetary disc: e.g., increasing the density by a factor of 2 could reduce the timescale by a factor of 30 for the formation of Jupiter. Such higher initial surface densities are likely to provide higher planetary mass than Jupiter

(Lissauer 1995; Pollack et al. 1996), consistent with the discovery of a number of extrasolar planets with such masses (see Marcy & Butler 2000; Jorissen et al. 2001). We thus conclude that the disc gaps and holes observed in RU Lup and CS Cha are consistent with the scenario that these are induced by a gas-giant planet formed at the ice condensation radius.

6. Conclusions

We present spectro-astrometric observations for 28 southern PMS stars. The structures detected in the position spectra include: (1) almost all the known binary companions in our sample (Sz 68, Sz 41, HO Lup, VW Cha, S CrA, and AS 205), (2) companion candidates which have not been detected by infrared speckle techniques (T CrA, MWC 300), (3) monopolar and bipolar jets (AS 353A, CS Cha), (4) a combination of a jet and stellar companion (R CrA), and (5) a combination of jets and a bow shock (VV CrA).

We succeeded to detect almost all the known binaries in our sample (6 out of 7) with separations of 0.1–1.5 arcsecs. The position of Hα emission in these objects are displaced primarily in the direction of the faint component, and their angular scales are consistent with those obtained by Bailey (1998b): 0.07–0.7 times as large as the binary separation. The displacement in the other features is much shorter than those in the Hα emission (0.02–0.05 times as large as binary separation) due to larger contribution of the continuum flux. All the observed displacements lie in the direction of the binary system, and these are explained by different spectra between the two binary components. Among the "spectro-astrometric" binary candidates, we confirm the time variation of the position angle in T CrA, consistent with binary motion.

From results in known binaries to date, we conclude that this technique should be able to detect binaries with separations down to ~10 milliarcsec. This detection limit is comparable to that of lunar occultations, although our technique can easily achieve better limits by observing a larger number of photons (Sect. 2), and is applicable for objects with any coordinate and binary position angles. The Hα profiles obtained for the components of the known binaries are strikingly similar to each other – similar linewidths and absorption features at similar velocities, results which support the scenario of core fragmentation for the mechanism of binary formation.

The Hα outflows observed by Bailey (1998b), Takami et al. (2001), and this work exhibit velocities coincident with the high-velocity components of the forbidden lines, suggesting that these are associated with jets close to the source. Among these objects, Z CMa and AS 353A show spatial scales more than 50 AU, and these are likely to be excited by shocks in the internal working surfaces. On the other hand, bipolar outflows in RU Lup and CS Cha exhibit much shorter spatial scales (1–5 AU), and the spatial scale and line profile in these objects suggest the presence of a heating mechanism other than shocks: e.g., X-ray or MHD-wave heating. From the observed spatial scales, flow velocities, and Hα luminosities of these flows, we estimate typical hydrogen number densities $\gtrsim 10^7$ cm^{-3}.

Our results in RU Lup (Takami et al. 2001) and CS Cha (this work) suggest the presence of disc gaps/holes at AU scales, consistent with the presence of a mid-infrared dip in their SEDs. The SEDs suggest that the outer radii of these gap and hole have temperatures of ~200 K, coincident with the ice condensation temperature (160–200 K). The constant temperature in these objects and a few more disc gap/hole candidates contrasts with the wide range for those in PMS binaries (30–600 K). The presence of such disc gaps/holes could be explained if a gas-giant planet formed at the ice condensation radius, clearing up the inside of the circumstellar disc by tidal interaction.

Appendix A: Expected luminosities for thermal radio emission

The fluxes of Hα and free-free emission per unit volume are described as follows (see Osterbrock 1989; Reynolds 1986):

$$4\pi j_{\mathrm{H}\alpha} = 3.5 \times 10^{-25} n_{\mathrm{p}} n_{\mathrm{e}} \qquad \text{erg cm}^{-3} \text{ s}^{-1} \tag{A.1}$$

$$4\pi j_{\nu} = 3.3 \times 10^{-38} n_{\mathrm{p}} n_{\mathrm{e}} \nu^{-0.1} \text{ erg cm}^{-3} \text{ s}^{-1} \text{ Hz}^{-1} \tag{A.2}$$

where n_{p} and n_{e} are the proton and electron densities, respectively; ν is the observed frequency for free-free emission. Throughout we assume an electron temperature of 10^4 K, plausible for either shock heating (see, e.g., Hartigan et al. 1994b), ambipolar diffusion (Safier 1993; Garcia et al. 2001), or UV photoionization (e.g., Osterbrock 1989) as a heating mechanism. We also assume that the Hα emission is produced via recombination, and the contribution from collisional excitation is negligible. Indeed, the transition level of Hα is too high to be excited thermally at the assumed temperature (Osterbrock 1989). Collisional excitation of Hα could occur in fast shocks, although the total Hα flux in these shocks may still be dominated by the "recombination plateau", which has a temperature of ~10^4 K and a much larger volume (e.g., by a factor of 10^3) than the region in which the line is collisionally excited (see Figs. 2–3 of Bacciotti & Eislöffel 1999).

Equations (A1) and (A2) show that free-free emission is proportional to that of Hα emission,

$$j_{3.6\mathrm{cm}} = 9.4 \times 10^{-15} j_{\mathrm{H}\alpha} \text{ Hz}^{-1}. \tag{A.3}$$

Table A.1 summarizes the observed parameters, and the estimated luminosities for free-free emission for the optically thin case. Note that the derived free-free luminosities are upper limits, since the radio thermal emission in YSOs are often optically thick (see Beltrán et al. 2001, and references therein).

Table A.1. Estimated radio luminosities.

object	R^a	EW^b	A_V	$L_{H\alpha}^c$	$S_{3.6\,cm}d^2$
	(mag)	(Å)	(mag)	($L_\odot$)	(mJy kpc^2)
RU Lup	9.99	29.7	1.28^d	1.4×10^{-2}	0.42
CS Cha	10.84	28.3	0.85^e	3.6×10^{-3}	0.11

^{a} Herbig & Bell (1988).
^{b} Sum for the blueshifted and redshifted emission in which positional displacement is observed.
^{c} Adopting the distances obtained by Wichmann et al. (1998).
^{d} Hughes et al. (1994).
^{e} Gauvin & Strom (1992).

Appendix B: Hydrogen density and opening angle of the Hα bipolar outflow

The total mass of the Hα emission line region and the Hα luminosity are described as follows:

$$M_{\text{out}} \sim \int m_p n_H \, \mathrm{d}V = \dot{M}_{\text{out}} l_{\text{out}}/v_{\text{out}} \tag{B.1}$$

$$L_{H\alpha} = 3.5 \times 10^{-25} \int n_p n_e \, \mathrm{d}V \quad \text{erg s}^{-1} \tag{B.2}$$

where m_p and n_H are the proton mass and the hydrogen number density, respectively; $\dot{M}_{\text{out}}$ is the mass loss rate; l_{out} and v_{out} are the spatial scale and the velocity of the observed outflow; n_p and n_e are the proton and electron number densities, respectively, in units of cm^{-3}; V is the volume of the Hα emission region. Equation (B.2) is derived adopting the recombination rate in Osterbrock (1989) assuming an electron temperature of 10^4 K (see Appendix A). We also assume that collisional excitation of Hα is negligible, since its transition level is too high to be thermally excited at the assumed temperature (Osterbrock 1989). Using Eqs. (B.1) and (B.2), the mean electron density is derived as follows:

$$
\begin{aligned}
\langle n_e \rangle &\equiv \frac{\int n_p n_e \, \mathrm{d}V}{\int n_p \, \mathrm{d}V} = \frac{L_{H\alpha}\,[\text{erg s}^{-1}]}{3.5 \times 10^{-25}} \frac{m_p v_{\text{out}}}{\dot{M}_{\text{out}} l_{\text{out}} \langle \chi_i \rangle} \\
&\sim 1.9 \times 10^{10} \, \langle \chi_i \rangle^{-1} \left(\frac{L_{H\alpha}}{1\,L_\odot} \right) \left(\frac{v_{\text{out}}}{100 \text{ km s}^{-1}} \right) \\
&\quad \times \left(\frac{\dot{M}_{\text{out}}}{10^{-8}\,M_\odot \text{ yr}^{-1}} \right)^{-1} \left(\frac{l_{\text{out}}}{1 \text{ AU}} \right)^{-1} \text{ cm}^{-3} \tag{B.3}
\end{aligned}
$$

where the mean ionization fraction is defined as $\langle \chi_i \rangle \equiv \left(\int n_p \, \mathrm{d}V \right) / \left(\int n_H \, \mathrm{d}V \right)$. From the Eq. (B.3), the mean hydrogen number density is derived as follows:

$$
\begin{aligned}
\langle n_H \rangle &\equiv \langle n_e \rangle / \langle \chi_i \rangle \\
&\sim 1.9 \times 10^{10} \, \langle \chi_i \rangle^{-2} \left(\frac{L_{H\alpha}}{1\,L_\odot} \right) \left(\frac{v_{\text{out}}}{100 \text{ km s}^{-1}} \right) \\
&\quad \times \left(\frac{\dot{M}_{\text{out}}}{10^{-8}\,M_\odot \text{ yr}^{-1}} \right)^{-1} \left(\frac{l_{\text{out}}}{1 \text{ AU}} \right)^{-1} \text{ cm}^{-3}. \tag{B.4}
\end{aligned}
$$

Next, we derive the typical opening angle of the flow assuming axisymmetric geometry and that the flow has zero width at its origin. The total mass in the flow is described as follows:

$$
\begin{aligned}
M_{\text{out}} &\sim \int \pi r_{\text{out}}^2 m_p n_H f_H \, \mathrm{d}l \\
&\sim 2\pi \langle r_{\text{out}}^2 \rangle l_{\text{out}} m_p \langle n_H \rangle \langle f_H \rangle \tag{B.5}
\end{aligned}
$$

where r_{out} is the radius (or half-width) of the flow at a certain distance from the star; $\langle r_{\text{out}}^2 \rangle$ is the mean square of the radius; f_H is the volume filling factor. On the other hand, the typical flow width $\langle d_{\text{out}} \rangle$ and opening angle $\langle \theta \rangle$ can be described as follows:

$$\langle d_{\text{out}} \rangle \equiv 2 \sqrt{\langle r_{\text{out}}^2 \rangle} \tag{B.6}$$

$$\langle \theta \rangle \equiv 2 \tan^{-1} \frac{\langle d_{\text{out}} \rangle}{2 l_{\text{out}}}. \tag{B.7}$$

Substituting Eqs. (B.1), (B.5), (B.6) to (B.7), $\langle \theta \rangle$ is derived as follows:

$$\langle \theta \rangle \sim 2 \tan^{-1} \sqrt{\frac{\dot{M}_{\text{out}}}{2\pi m_p \langle n_H \rangle v_{\text{out}} l_{\text{out}}^2 \langle f_H \rangle}}. \tag{B.8}$$

References

Abt, H. A., Gomez, A. E., & Levy, S. G. 1990, ApJS, 74, 551
Alencar, S. H. P., & Batalha, C. 2002, ApJ, 571, 378
Andre, P., Deeney, B. D., Phillips, R. B., & Lestrade, J. 1992, ApJ, 401, 667
Anglada, G. 1996, Radio Emission from the Stars and the Sun, ASP Conf. Ser., 93, 3
Bacciotti, F., & Eislöffel, J. 1999, A&A, 342, 717
Bacciotti, F., Mundt, R., Ray, T. P., et al. 2000, ApJ, 537, L49
Bailey, J. A. 1998a, Proc. SPIE, 3355, 932
Bailey, J. 1998b, MNRAS, 301, 161
Bastien, P. 1985, ApJS, 59, 277
Bate, M. R., Bonnell, I. A., Clarke, C. J., et al. 2000, MNRAS, 317, 773
Beltrán, M. T., Estalella, R., Anglada, G., Rodríguez, L. F., & Torrelles, J. 2001, AJ, 121, 1556
Beristain, G., Edwards, S., & Kwan, J. 2001, ApJ, 551, 1037
Bertout, C., Robichon, N., & Arenou, F. 1999, A&A, 352, 574
Binette, L., Cabrit, S., Raga, A., & Cantó, J. 1999, A&A, 346, 260
Boss, A. P. 1995, Science, 267, 360
Boss, A. P. 2000, ApJ, 536, L101
Boss, A. P., & Yorke, H. W. 1993, ApJ, 411, L99
Boss, A. P., & Yorke, H. W. 1996, ApJ, 469, 366
Cabrit, S., Edwards, S., Strom, S. E., & Strom, K. M. 1990, ApJ, 354, 687
Calvet, N. 1997, Herbig-Haro Flows and the Birth of Stars, IAU Symp., 182, 417
Calvet, N., & Gullbring, E. 1998, ApJ, 509, 802
Calvet, N., Hartmann, L., & Strom, S. E. 2000, Protostars and Planets IV, 377
Claria, J. J. 1974, A&A, 37, 229
Corcoran, M., & Ray, T. P. 1997, A&A, 321, 189
Corporon, P., & Lagrange, A.-M. 1999, A&AS, 136, 429
Curiel, S., Raga, A., Raymond, J., Noriega-Crespo, A., & Canto, J. 1997, AJ, 114, 2736
de Geus, E. J., & Burton, W. B. 1991, A&A, 246, 559
de Zeeuw, P. T., Hoogerwerf, R., de Bruijne, J. H. J., Brown, A. G. A., & Blaauw, A. 1999, AJ, 117, 354
Dougados, C., Cabrit, S., Lavalley, C., & Ménard, F. 2000, A&A, 357, L61

Drissen, L., Bastien, P., & St.-Louis, N. 1989, AJ, 97, 814

Duchêne, G., Monin, J.-L., Bouvier, J., & Ménard, F. 1999, A&A, 351, 954

Duquennoy, A., & Mayor, M. 1991, A&A, 248, 485

Dutrey, A., Guilloteau, S., & Simon, M. 1994, A&A, 286, 149

Edwards, S., Strom, S. E., Hartigan, P., et al. 1993, AJ, 106, 372

Eislöffel, J., Mundt, R., Ray, T. P., & Rodriguez, L. F. 2000, Protostars and Planets IV, 815

Fischer, D. A., & Marcy, G. W. 1992, ApJ, 396, 178

Garcia, P. J. V., Ferreira, J., Cabrit, S., & Binette, L. 2001, A&A, 377, 589

Garcia, P. J. V., Thiébaut, E., & Bacon, R. 1999, A&A, 346, 892

Gauvin, L. S., & Strom, K. M. 1992, ApJ, 385, 217

Ghez, A. M., Neugebauer, G., & Matthews, K. 1993, AJ, 106, 2005

Ghez, A. M., Weinberger, A. J., Neugebauer, G., Matthews, K., & McCarthy, D. W. 1995, AJ, 110, 753

Ghez, A. M., McCarthy, D. W., Patience, J. L., & Beck, T. L. 1997a, ApJ, 481, 378

Ghez, A. M., White, R. J., & Simon, M. 1997b, ApJ, 490, 353

Graham, J. A. 1992, PASP, 104, 479

Guilloteau, S., Dutrey, A., & Simon, M. 1999, A&A, 348, 570

Halbwachs, J. L., Arenou, F., Mayor, M., Udry, S., & Queloz, D. 2000, A&A, 355, 581

Hale, A. 1994, AJ, 107, 306

Hamann, F. 1994, ApJS, 93, 485

Hartigan, P., Edwards, S., & Ghandour, L. 1995, ApJ, 452, 736

Hartigan, P., Strom, K. M., & Strom, S. E. 1994a, ApJ, 427, 961

Hartigan, P., Morse, J. A., & Raymond, J. 1994b, ApJ, 436, 125

Hartmann, L., Edwards, S., & Avrett, E. 1982, ApJ, 261, 279

Hayashi, C. 1981, Fundamental Problems in the Theory of Stellar Evolution, IAU Symp., 93, 113

Herbig, G. H., & Bell, K. R. 1988, Lick Observatory Bulletin, Santa Cruz: Lick Observatory, – c1988

Herbig, G. H., & Jones, B. F. 1983, AJ, 88, 1040

Hillenbrand, L. A., Strom, S. E., Vrba, F. J., & Keene, J. 1992, ApJ, 397, 613

Hirth, G. A., Mundt, R., & Solf, J. 1997, A&AS, 126, 437

Hughes, J., Hartigan, P., Krautter, J., & Kelemen, J. 1994, AJ, 108, 1071

Jensen, E. L. N., & Mathieu, R. D. 1997, AJ, 114, 301

Jorissen, A., Mayor, M., & Udry, S. 2001, A&A, 379, 992

Kepner, J., Hartigan, P., Yang, C., & Strom, S. 1993, ApJ, 415, L119

Köhler, R., Kunkel, M., Leinert, C., & Zinnecker, H. 2000, A&A, 356, 541

Königl, A., & Pudritz, R. E. 2000, Protostars and Planets IV, 759

Koresko, C. D., Herbst, T. M., & Leinert, C. 1997, ApJ, 480, 741

Lamzin, S. A., Bisnovatyi-Kogan, G. S., Errico, L., et al. 1996, A&A, 306, 877

Lavalley-Fouquet, C., Cabrit, S., & Dougados, C. 2000, A&A, 356, L41

Leinert, C., Richichi, A., & Haas, M. 1997, A&A, 318, 472

Leinert, C., Zinnecker, H., Weitzel, N., et al. 1993, A&A, 278, 129

Lissauer, J. J. 1987, Icarus, 69, 249

Lissauer, J. J. 1995, Icarus, 114, 217

Liu, M. C., Graham, J. R., Ghez, A. M., et al. 1996, ApJ, 461, 334

Lubow, S. H., & Artymowicz, P. 2000, Protostars and Planets IV, 731

Marcy, G. W., & Butler, R. P. 2000, PASP, 112, 137

Marcy, G. W., Cochran, W. D., & Mayor, M. 2000, Protostars and Planets IV, 1285

Marraco, H. G., & Rydgren, A. E. 1981, AJ, 86, 62

Marsh, K. A., & Mahoney, M. J. 1992, ApJ, 395, L115

Marsh, K. A., & Mahoney, M. J. 1993, ApJ, 405, L71

Martin, S. C. 1996, ApJ, 473, 1051

Mathieu, R. D., Ghez, A. M., Jensen, E. L. N., & Simon, M. 2000, Protostars and Planets IV, 703

Ménard, F., & Bastien, P. 1992, AJ, 103, 564

Monin, J.-L., Menard, F., & Duchêne, G. 1998, A&A, 339, 113

Muzerolle, J., Calvet, N., & Hartmann, L. 1998, ApJ, 492, 743

Muzerolle, J., Calvet, N., & Hartmann, L. 2001, ApJ, 550, 944

Najita, J. R., Edwards, S., Basri, G., & Carr, J. 2000, Protostars and Planets IV, 457

Osterbrock, D. E. 1989, Astrophysics of Gaseous Nebulae and Active Galactic Nuclei (Univ. Science Books, Mill Valley)

Padgett, D. L., Strom, S. E., & Ghez, A. 1997, ApJ, 477, 705

Palla, F., & Stahler, S. W. 1999, ApJ, 525, 772

Petr, M. G., Coude Du Foresto, V., Beckwith, S. V. W., Richichi, A., & McCaughrean, M. J. 1998, ApJ, 500, 825

Pirzkal, N., Spillar, E. J., & Dyck, H. M. 1997, ApJ, 481, 392

Poetzel, R., Mundt, R., & Ray, T. P. 1989, A&A, 224, L13

Pollack, J. B., Hubickyj, O., Bodenheimer P., et al. 1996, Icarus, 124, 62

Prato, L., & Simon, M. 1997, ApJ, 474, 455

Prosser, C. F., Stauffer, J. R., Hartmann, L., et al. 1994, ApJ, 421, 517

Ray, T. P., Mundt, R., Dyson, J. E., Falle, S. A. E. G., & Raga, A. C. 1996, ApJ, 468, L103

Reipurth, B., Pedrosa, A., & Lago, M. T. V. T. 1996, A&AS, 120, 229

Reipurth, B., & Zinnecker, H. 1993, A&A, 278, 81

Reynolds, S. P. 1986, ApJ, 304, 713

Richichi, A., Leinert, C., Jameson, R., & Zinnecker, H. 1994, A&A, 287, 145

Richichi, A., Calamai, G., Leinert, C., Stecklum, B., & Trunkovsky, E. M. 1996, A&A, 309, 163

Richichi, A., Calamai, G., Leinert, C., & Stecklum, B. 1997, A&A, 322, 202

Safier, P. N. 1993, ApJ, 408, 115

Shang, H., Glassgold, A. E., Shu, F. H., & Lizano, S. 2002, ApJ, 564, 853

Shu, F. H., Najita, J. R., Shang, H., & Li, Z.-Y. 2000, Protostars and Planets IV, 789

Simon, M., Ghez, A. M., Leinert, C., et al. 1995, ApJ, 443, 625

Solf, J., Böhm, K.-H., & Raga, A. C. 1986, ApJ, 305, 795

Stahler, S. W., & Walter, F. M. 1993, Protostars and Planets III, 405

Stevenson, D. J., & Lunine, J. I. 1988, Icarus, 75, 146

Strom, K. M., Strom, S. E., Edwards, S., Cabrit, S., & Skrutskie, M. F. 1989, AJ, 97, 1451

Takami, M., Bailey, J., Gledhill, T. M., Chrysostomou, A., & Hough, J. H. 2001, MNRAS, 323, 177

Takami, M., Chrysostomou, A., Bailey, J., et al. 2002, ApJ, 568, L53

Takeuchi, T., Miyama, S. M., & Lin, D. N. C. 1996, ApJ, 460, 832

White, R. J., & Ghez, A. M. 2001, ApJ, 556, 265

Wichmann, R., Bastian, U., Krautter, J., Jankovics, I., & Rucinski, S. M. 1998, MNRAS, 301, L39

Wilking, B. A., Greene, T. P., Lada, C. J., Meyer, M. R., & Young, E. T. 1992, ApJ, 397, 520